

## Supporting Information

### UV-driven overall water splitting using unsupported gold nanoparticles as photocatalyst

Bining Tian<sup>b,c,\*</sup>, Qin Lei<sup>a,\*</sup>, Bin Tian<sup>a</sup>, Wenxing Zhang<sup>a</sup>, Yanxia Cui<sup>a</sup>, & Yue Tian<sup>a,c</sup>

<sup>a</sup> Key Lab of Advanced Transducers and Intelligent Control System of Ministry of Education, College of Physics and Optoelectronics, Taiyuan University of Technology, Taiyuan 030024, China

<sup>b</sup> Department of Physics, Dalian Maritime University, Dalian 116600, China

<sup>c</sup> Molecular Foundry, Lawrence Berkeley National Laboratory, Berkeley, CA 94720, USA

\* These authors contributed equally to this work. Correspondence and requests for materials should be addressed to Y.T. (email: [tianyue@tyut.edu.cn](mailto:tianyue@tyut.edu.cn), [yuetian@lbl.gov](mailto:yuetian@lbl.gov)).

## **Experimental section**

### **Methods**

**Materials.** All of the chemicals of analytical grade used in this work were purchased from Aladdin Chemical Co. (China) and were used as received without further purification. De-ionized (DI) water with a specific resistance of 18.2 M $\Omega$ ·cm was obtained by reverse osmosis followed by ion-exchange and filtration (RFD 250NB, Toyo Seisakusho Kaisha, Ltd., Japan).

#### **Preparation of Au nanoparticles (Au NPs)**

Au NPs were prepared by a citrate-reduction method as reported before<sup>1</sup>. Briefly, 50 mL 0.01% chloroauric acid solution was heated to 95 °C. Then, a certain amount of 1% citrate sodium was injected into the boiling chloroauric acid solution fast. Keeping stirring at 95 °C for another 20 min, the Au NPs were collected via centrifugation and washing with DI water. Finally, the as-prepared Au NPs were re-dispersed into DI water with the concentration of 1 mg/mL for further use.

#### **Preparation of Au/Pt nanocomposites**

Pt NPs were deposited on the surface of Au NPs via an in-situ reduction. In a typical procedure, 1 mL of the as-prepared Au NPs solution was added into 100 mL of triethanolamine aqueous solution (TEOA-H<sub>2</sub>O, 10%, v/v, pH = 11) in a sealed Pyrex flask (170 ml) with a flat window (an efficient irradiation area of 10.2 cm<sup>2</sup>) and a silicone rubber septum for sampling. Then, the certain amounts of K<sub>2</sub>PtCl<sub>6</sub> solution and Eosin Y (EY) were added into the above Au NPs solution under vigorous stirring. After being degassed by bubbling Ar gas for 30 min. the mixed solution was irradiated under a 300-W Xenon lamp equipped with a 420 nm cutoff filter for 2h. The sample was centrifuged and washed with pure water and anhydrous ethanol to remove the

residual TEOA and EY completely. Finally, the as-prepared Au/Pt NPs were re-dispersed into DI water for further use.

### **Characterizations**

X-ray diffraction (XRD) data were obtained on a Rigaku B/Max-RB powder diffractometer using Cu K $\alpha$  radiation ( $\lambda = 1.5406\text{\AA}$ ) at a scanning rate of  $2^\circ$  per min over a  $2\theta$  range of  $10\text{--}80^\circ$  with a step size of  $0.017^\circ$ . Transmission electron microscopy (TEM) and high-resolution TEM (HRTEM) images were recorded using a Tecnai-G2-F30 field emission transmission electron microscope with an accelerating voltage of 300 kV. SEM images were acquired on a Zeiss Gemini Ultra-55 analytical field emission scanning electron microscope operating in transmission mode. X-ray photoelectron spectroscopy (XPS) analysis was recorded on a VG Scientific ESCALAB 210-XPS with a Mg K $\alpha$  X-ray resource. The binding energy C 1s peak from surface adventitious carbon (284.8 eV) was adopted as a reference for the binding energy measurements. The diffuse reflectance UV-visible spectra of the samples were measured by a PerkinElmer Lambda 900 UV/VIS/NIR spectrometer equipped with an integrating sphere covered with BaSO $_4$  as the reference. Ultraviolet photoemission measurements (UPS) were carried out in an ultra-high-vacuum ESCALAB 210 multianalysis system (base pressure  $1.0\times 10^{-10}$  mbar) from Thermo VG Scientific. Photoelectrons were excited by means of a helium lamp by using the He I (21.22 eV) excitation lines.

### **Activity and Stability Measurement of Catalysts**

The photocatalytic reactions of the Au and Au/Pt photocatalysts were carried out in a top-irradiation-type Pyrex glass photoreactor connected to a closed gas-circulation and evacuation system under the 250 W medium pressure mercury vapor lamp. Typically, 1 mg of the

photocatalysts was dispersed into 100 ml DI water under magnetic stirring. The reaction cell was irradiated by the 250 W medium pressure mercury vapor lamp after being thoroughly degassed to remove air by Ar. The photocatalytic gas evolution rate was analyzed using an online SP-6890 gas chromatograph (GC, TCD detector, 5 Å molecular sieve columns and Ar carrier). The stability tests of catalysts were performed for 32 h, including 4 runs under the same experimental conditions as activity measurement. After each run reaction, the catalyst was separated by centrifugation and washing thoroughly by DI water for another run reaction.

### **Electrochemical Measurements**

All the electrochemical measurements were measured on an electrochemical analyzer (CHI660E) in a typical three-electrode cell (a Pt counter electrode, a reference electrode of saturated calomel electrode (SCE) and a working electrode). The working electrodes were prepared by drop-coating sample suspensions directly onto the precleaned indium tin oxide glass (ITO glass) surface. In detail, catalysts solution (2 mL) was ultrasonic treatment for 30 min. 75  $\mu\text{L}$  sample mixture was drop-coated onto the precleaned indium tin oxide (ITO) glass or glassy carbon electrode (GCE) surface ( $1\text{ cm}^2$ ) and was air-dried (loaded about  $0.15\text{ mg}\cdot\text{cm}^{-2}$ ) before measurement. The supporting electrolyte was  $0.5\text{ mol}\cdot\text{L}^{-1}\text{ H}_2\text{SO}_4$  aqueous solutions. The interfacial charge transfers of catalysts were exposed using the electrochemical impedance spectroscopies (EIS) in the frequency range of  $10^{-2}$  to  $10^6$  Hz with 10 mV sinusoidal perturbations. A 250W medium pressure mercury vapor lamp was used for excitation.

### **Theoretical calculation**

To further confirm our conclusion, the calculation of the extinction (as an addition of absorption and scattering) spectra of Au NPs was carried out based on the finite-difference time-

domain (FDTD) analysis method.<sup>2</sup> A gold sphere with the refractive indices obtained from the Johnson and Christy measurement is placed in water with the refractive index of 1.33.<sup>3</sup> A sufficient large fit coefficient is used to provide a good fit to the sampled gold refractive indices over the investigated bandwidth between 200 nm and 600 nm. Two major extinction peaks are produced by the gold sphere, as displayed in Fig. S20. One locates at the visible range (around 525 nm) and the other is present at the UV range (between 200 and 400 nm). As well known, the peak at the visible range is the SPR absorption having the dipolar nature. Gold at the UV range no longer possesses the noble metal property, instead it appears like a semiconductor (in other words, a lossy dielectric) due to strong interband electron transitions. Thus, the peak at the UV range is produced due to dielectric particle scattering. Moreover, it is seen clearly that with the increase of the particle diameter, both the two peaks red-shift, in agreement with the experimental results. The amplitude and phase distributions for the gold sphere with 25 nm diameter at the two peaks (523 nm and 249 nm) are plotted in Fig. S21(A-B) and (C-D), respectively. One sees that in Fig. S21 (A), due to the excitation of SPR, the field intensity around the gold particle becomes much greater than that in the background of water. On the contrary, the scattering effect due to semiconductor-type lossy dielectric particle is relatively weaker, resulting in the field surrounding the gold particle is only slightly stronger than that in the background as shown Fig. S21(B). Besides, the phase distributions at the two peaks are also distinct from each other apparently. In Fig. S21 (C), the field inside the particle experiences  $\pi$  shifts in phase from that outside of the particle that is a feature of the dipolar mode. But in Fig. S21 (D), the fields inside and outside of the particle are almost in phase since the scattering effect is generated due to the difference in refractive index (at the UV range, such difference is very small). Therefore, we can conclude that the SPR effect has no contribution to the photocatalytic activity of Au NPs. We also used the DFT code Dmol3 to calculate the molecular orbital and spectra of gold cluster (Au<sub>20</sub>) in tetrahedral shape along [111] crystal direction as an ideal model, where LSDA functional and all-electron scheme are applied during the calculation. As shown in Fig. S22, a stable structure with the strongest transition of 3.3 eV energy gap is obtained, which is close to the experimental result (3.51 eV) and the energy level positions are suitable for water splitting. In addition, TDDFT calculation reveals the transition at 3.3 eV have the highest activity for chemical reaction (Fig. S23).

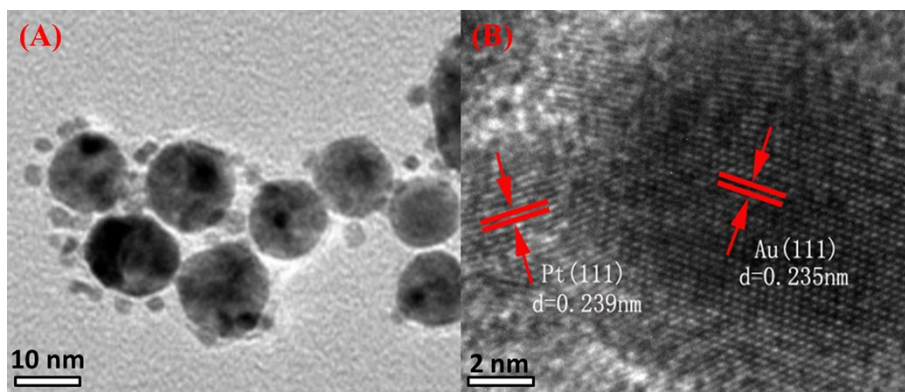


**Figure S1.** (A) TEM and HRTEM images of Au/Pt nanohybrids.

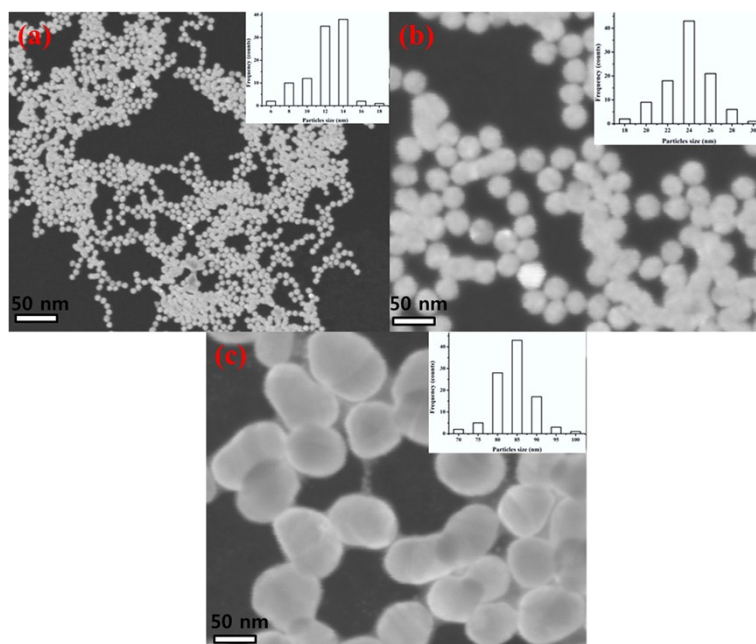


**Figure S2.** SEM images of Au NPs with different sizes: (a) 13nm, (b) 25nm and (c) 80 nm, and statistically relevant number of particles, respectively (insets).

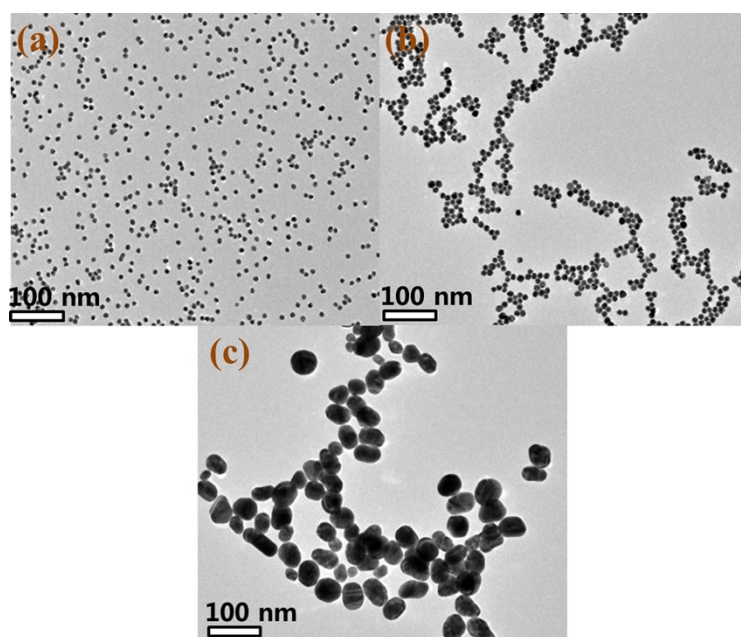


**Figure S3.** TEM images of Au NPs prepared by using different amount of sodium citrate solution

(a) 1.5 mL, (b) 1 mL and (c) 0.25 mL.

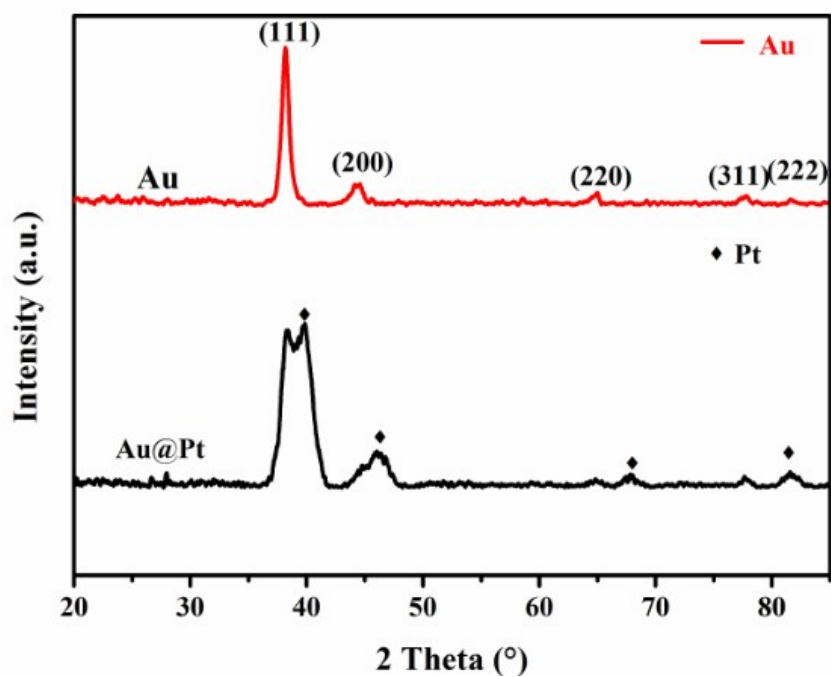
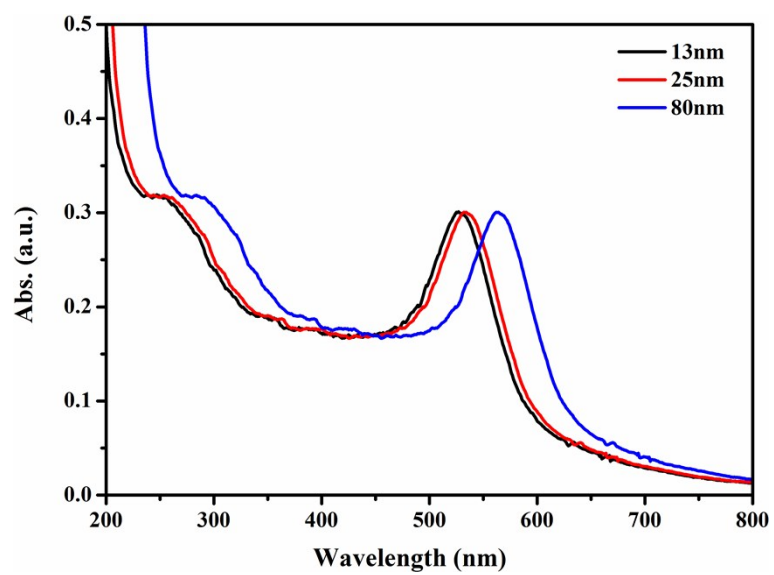
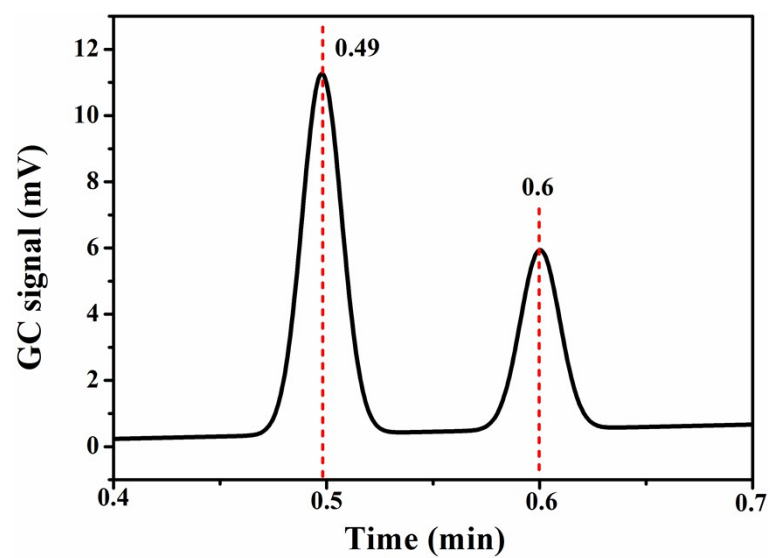


Figure S4. XRD patterns of Au and Au/Pt photocatalysts.



**Figure S5.** Ultraviolet-visible absorption spectra of Au NPs in aqueous solution.



**Figure S6.** A typical gas chromatograph trace of evolved hydrogen and gas chromatograph signal peaks at 0.49 and 0.6 corresponding to H<sub>2</sub> and O<sub>2</sub> evolution, respectively.

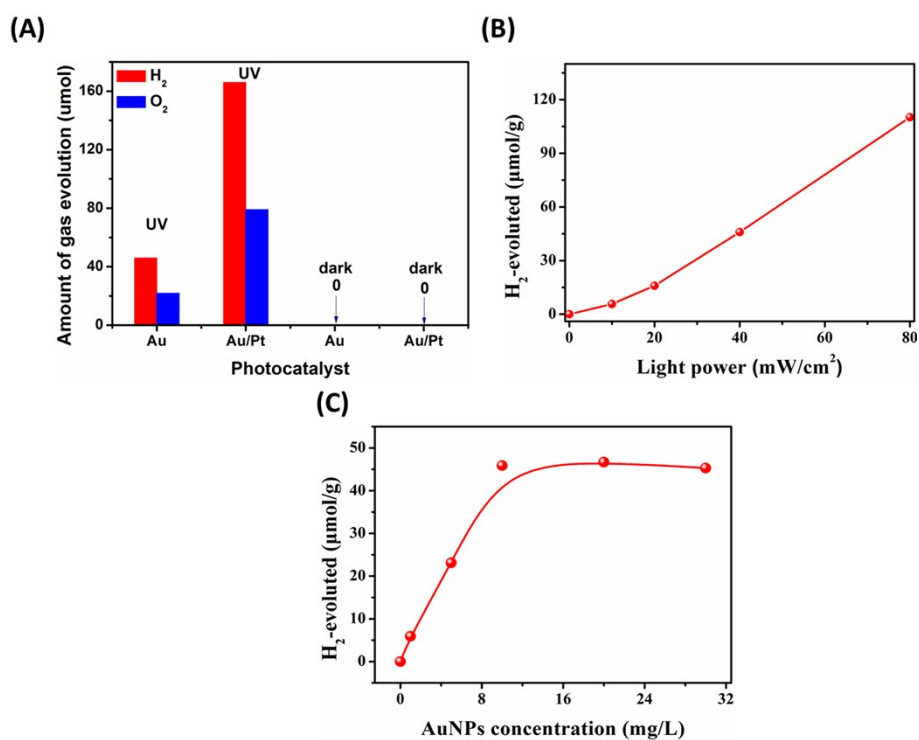


**Figure S7.** (A) Water splitting activity of Au and Au/Pt NPs under UV irradiation and dark condition, (B) Production of hydrogen from Au NPs as a function of light intensity, (C) Dependence of hydrogen evolution activity on the amount of Au NPs. The light source is 250 W medium pressure mercury vapor lamp and reaction time is 8 hours.

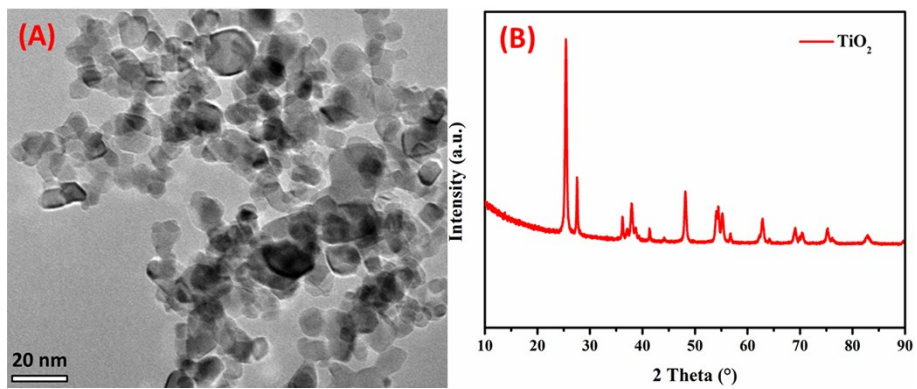


**Figure S8.** TEM (A) image and XRD (B) pattern of pristine TiO<sub>2</sub> (P25).

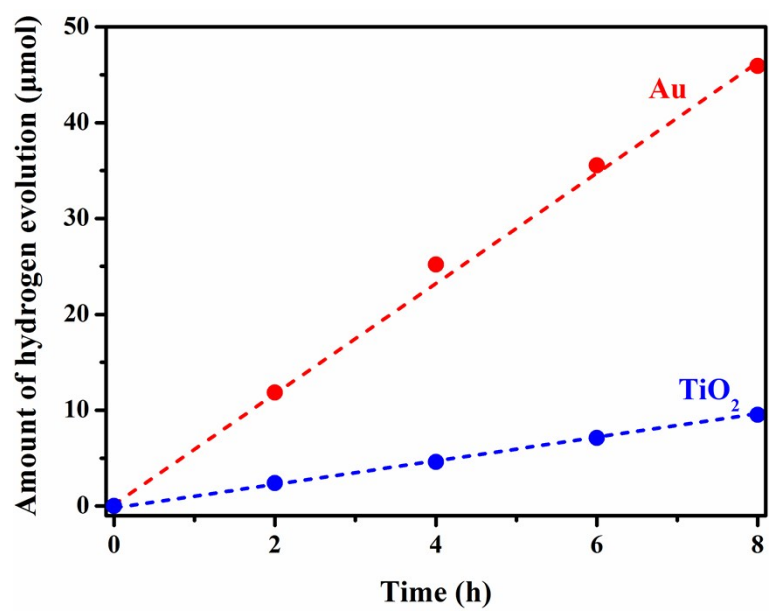


**Figure S9.** The comparison of hydrogen evolution over Au and TiO<sub>2</sub> NPs.

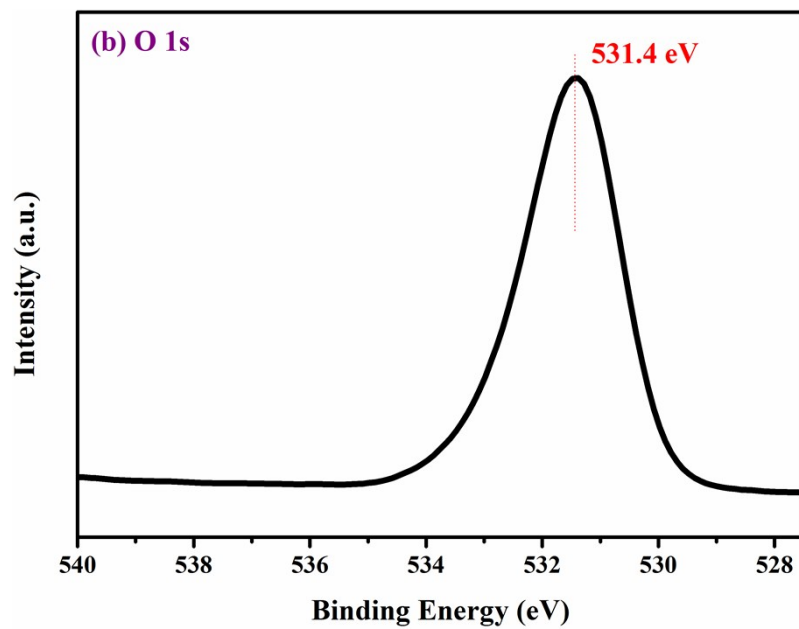


**Figure S10.** XPS spectrum of O 1s spectrum of Au NPs.

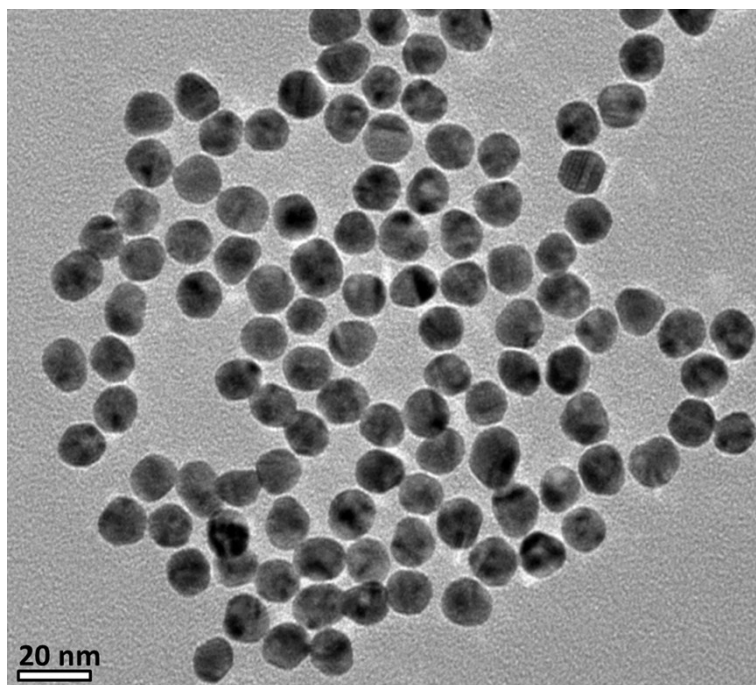


**Figure S11.** TEM image of Au NPs after the photoreaction.

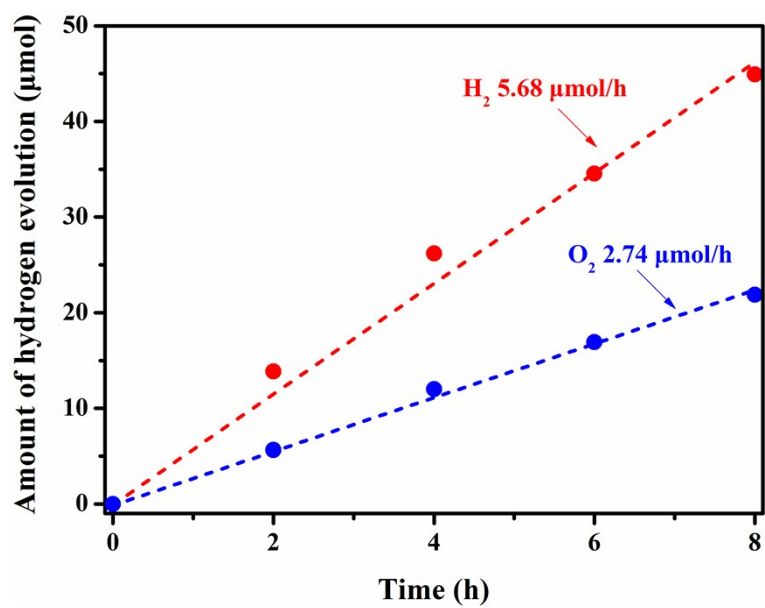


**Figure S12.** The hydrogen evolution activity of Au NPs annealed at 600 °C for 2h.

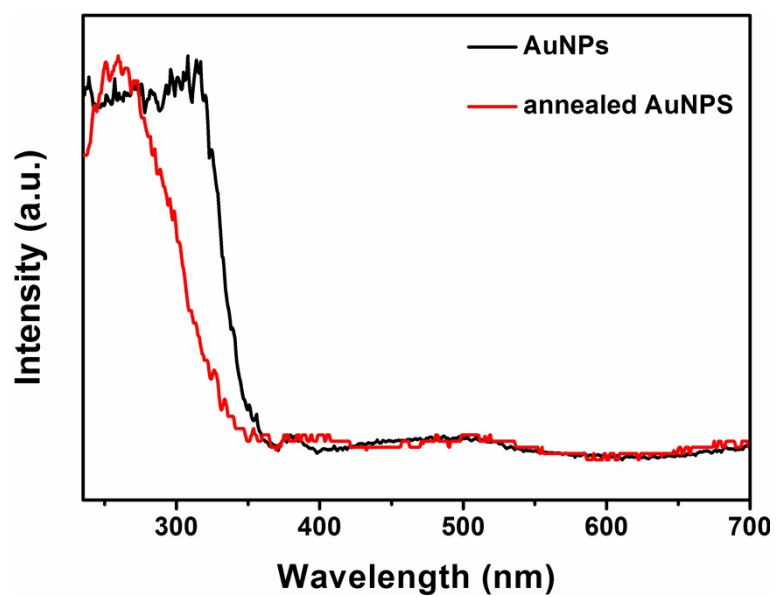


**Figure S13.** The UV-vis spectra of the pristine and annealed Au NPs.

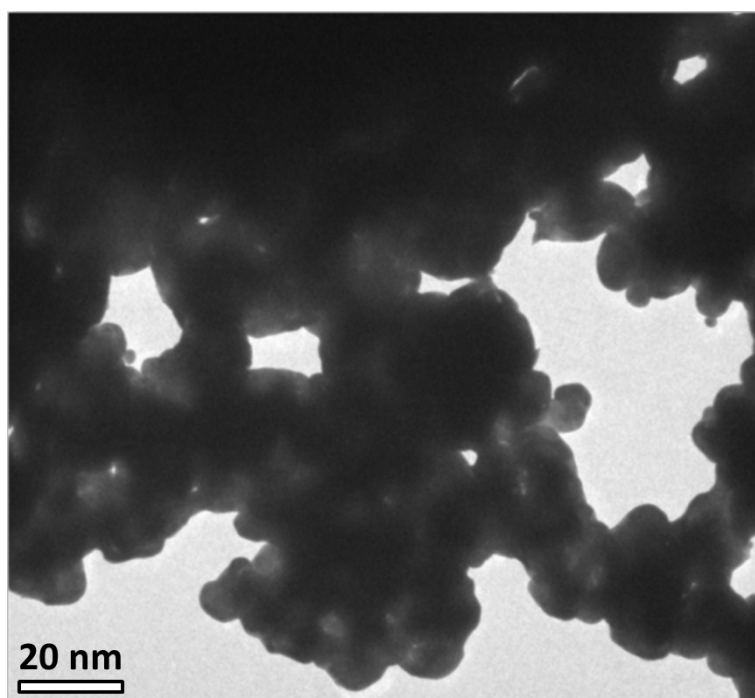


**Figure S14.** TEM image of Au NPs after being annealed at 600 °C for 2h.

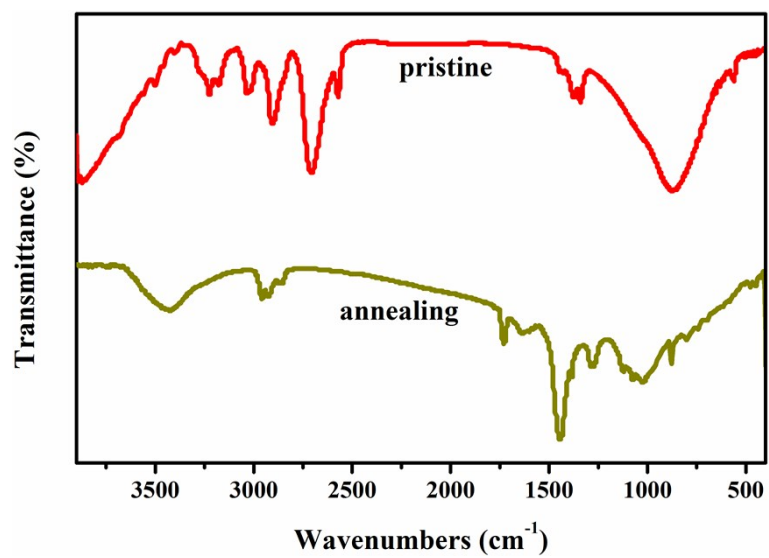


**Figure S15.** Fourier transformation infrared spectra (FTIR) of Au NPs.

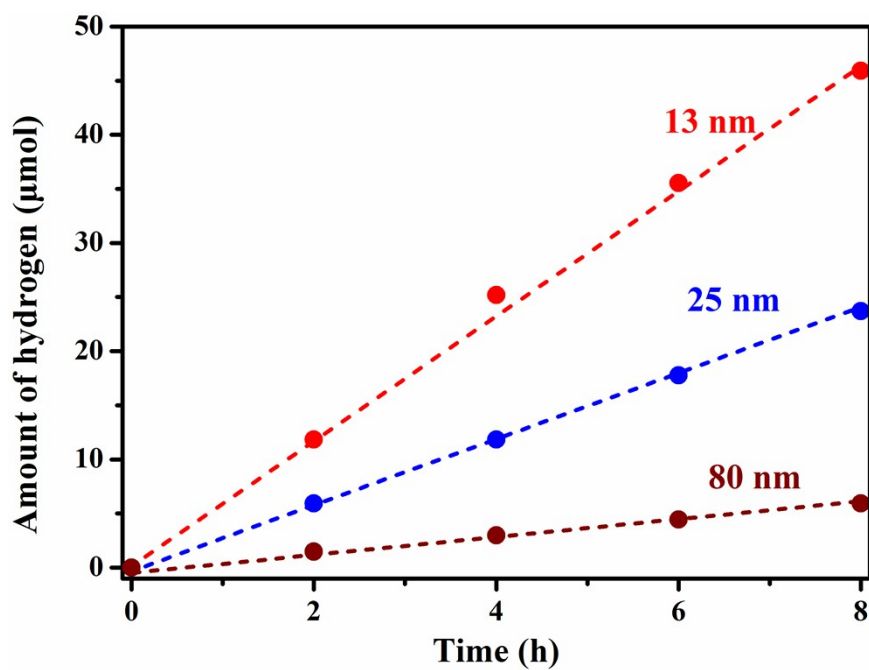


**Figure S16.** The time course of H<sub>2</sub> evolution from water over Au NPs photocatalyst with different sizes. It can be observed that the photocatalytic activity decreases with the increase of Au NPs diameter because there are much more active sites for chemical reaction at small size level compared to the big size particles

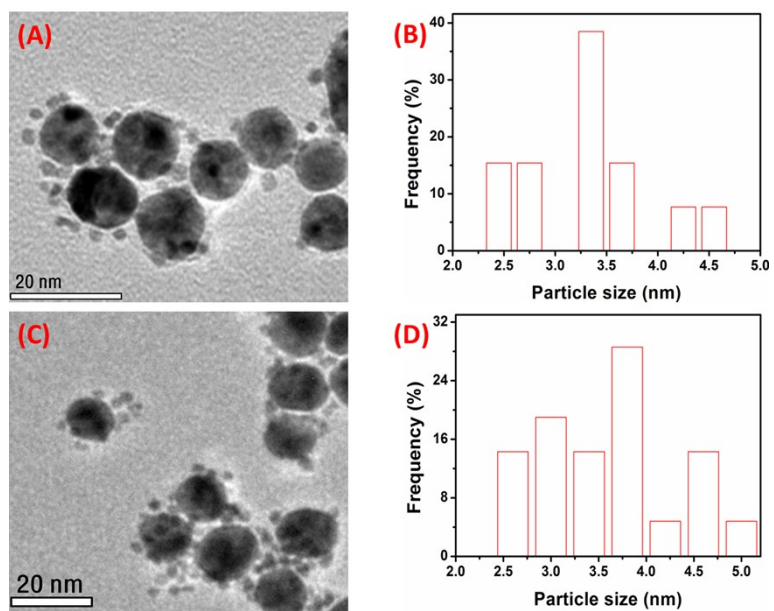


**Figure S17.** TEM images and size distribution of Au/Pt NPs before (A, B) and after (C, D) UV irradiation.

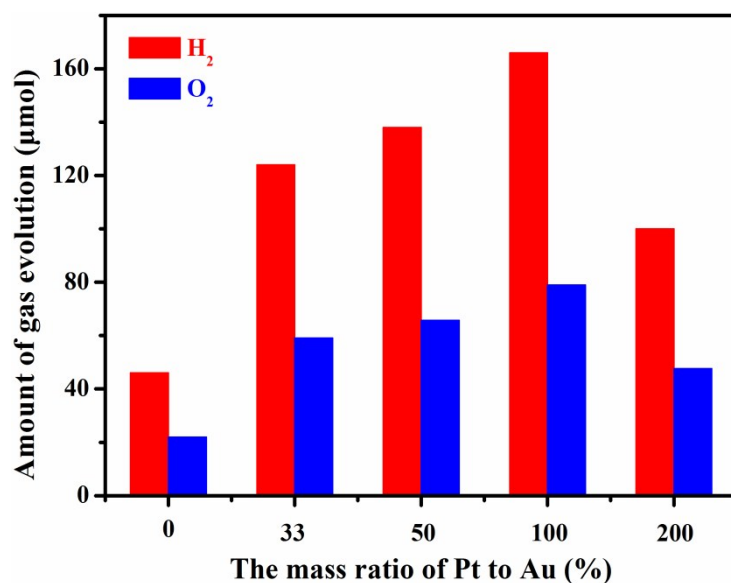


**Figure S18.** The influence of Pt loading amount on the gas evolution in Au/Pt photocatalysts. The gas production rates increases with the Pt load until a maximum at around 100% (weight ratio) and decreases with further Pt loading. Such an activity decrease should be associated with the nucleation, at too-high Pt loads, of independent Pt NPs outside the Au NPs surface. Such independent nanocrystals are much less effective in promoting the water-splitting reaction but still scattered photons, thus decreasing the light absorption on Au NPs. The observation of such an optical shielding effect confirms that an intimate interface between Au and Pt is a key to promote the photocatalytic hydrogen generation.<sup>4-6</sup>

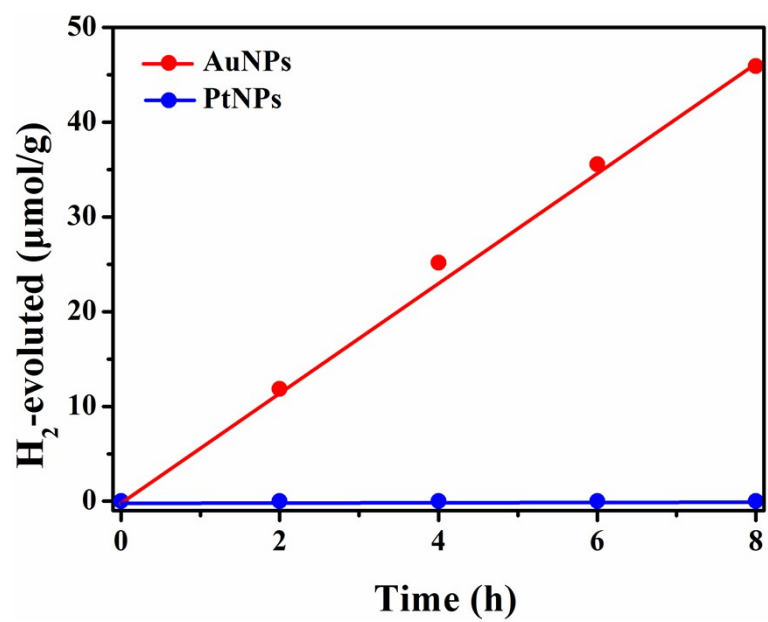


**Figure S19.** Photocatalytic activity of Au and Pt NPs under UV light irradiation. The light source is 250W Hg lamp.

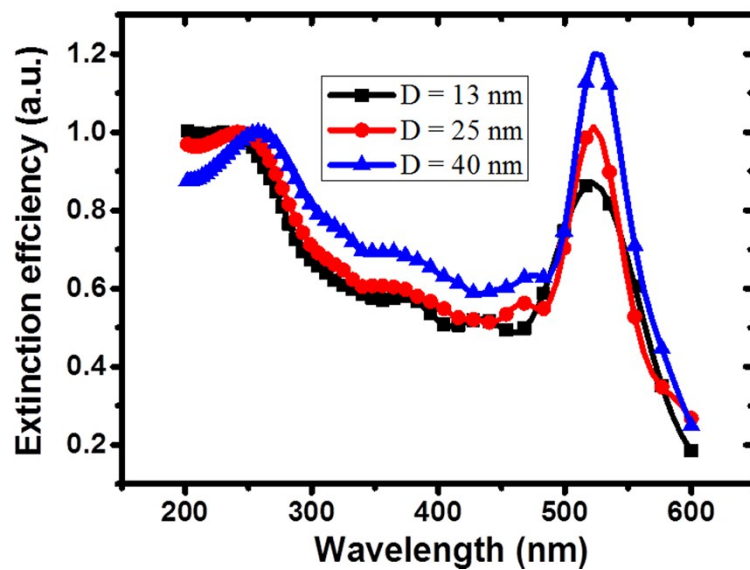


**Figure S20.** The extinction spectra of different gold particles in water. D = 13 nm, 25 nm, and 40 nm.

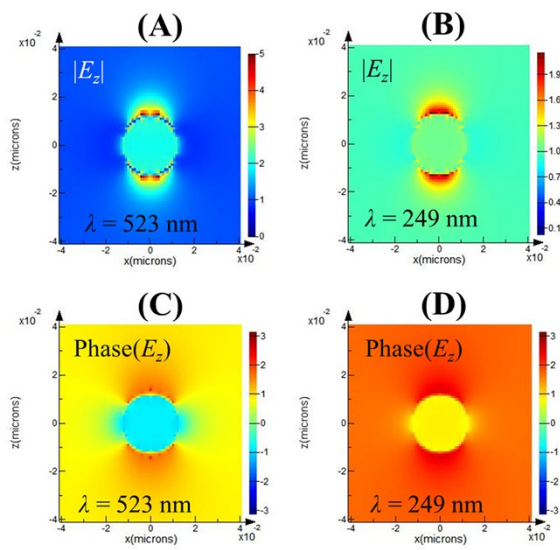


**Figure S21.** The cross section profiles of amplitude (A-B) and phase (C-D) of the major electric field component ( $E_z$ ) at the two extinction peaks when a gold particle with diameter of 25 nm is dispersed in water. The cross section is taken at the  $x$ - $z$  plane when  $y = 0$ . In the simulation, the light with electric field polarized along  $z$  direction incident on the gold particle along  $y$  direction forwardly.

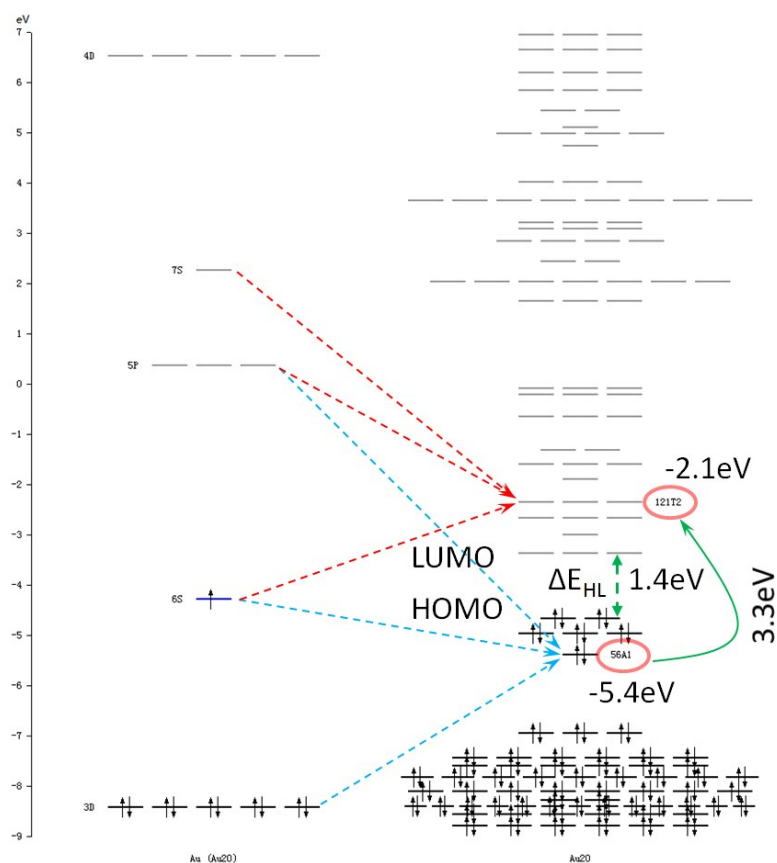


**Figure S22.** Comparison between the electronic configuration of gold atom and that of gold cluster Au<sub>20</sub>. The energy gap from HOMO to LUMO is illustrated as  $\Delta E_{HL}$ . ‘3D’, ‘6S’, ‘5P’, ‘7S’ and ‘4D’ are atomic orbital labels. ‘56A1’ and ‘121T2’ are the molecular orbital labels corresponding to the strongest transition in the UV/Vis spectra of Supplementary Figure 14. The black arrows show the occupation of electrons with spin (up and down).

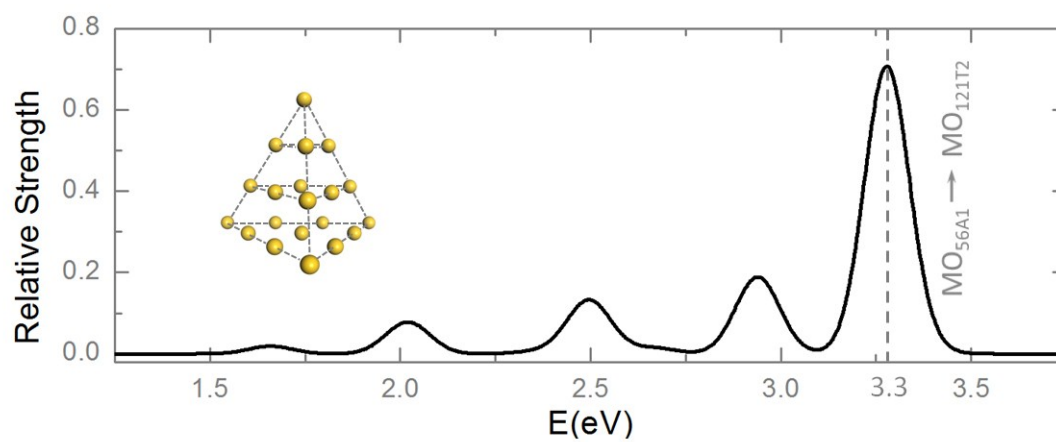


**Figure S23.** UV/Vis spectra of tetrahedral gold cluster Au<sub>20</sub> from TDDFT calculation of excited states. The strongest transition from molecular orbital ‘56A1’ to ‘121T2’ is marked. The inset is the illustration of Au<sub>20</sub> geometry.

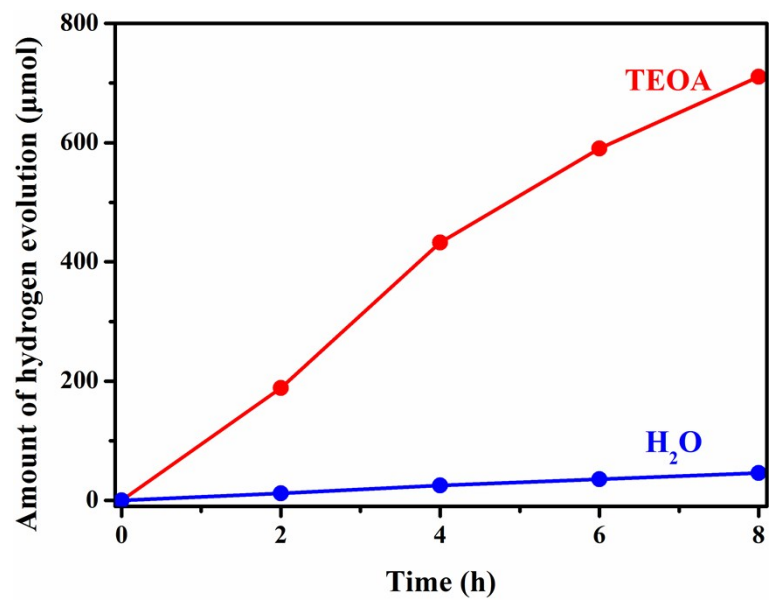


**Figure S24.** The time course of H<sub>2</sub> evolution from water in TEOA and H<sub>2</sub>O system with Au NPs.

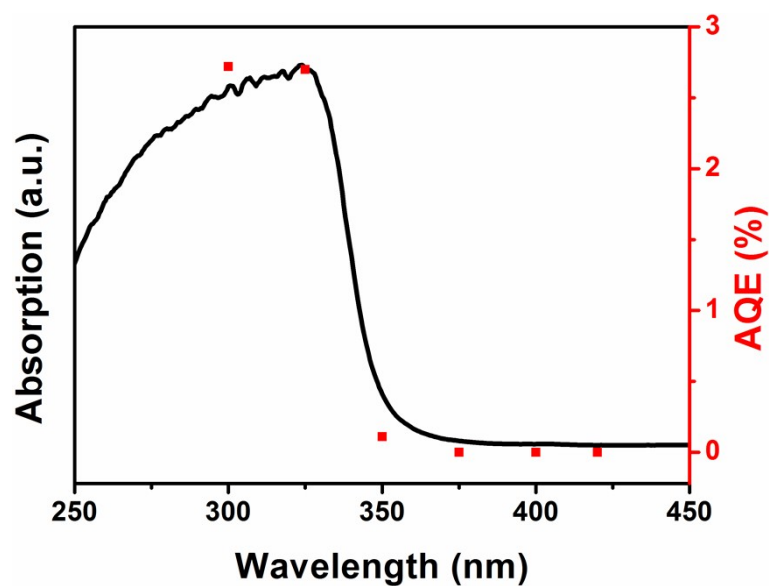


**Figure S25.** Wavelength-dependent AQE (red dots) of hydrogen evolution over the Au/Pt NPs irradiated by UV LEDs with wavelengths of 300, 325, 350, 375, 400 and 420 nm. The solution is 10% TEOA water solution.

## Notes and references

1. P. X. Zhao, N. Li and D. Astruc, *Coordin. Chem. Rev.*, 2013, **257**, 638–665.
2. Theory and computation of electromagnetic fields by jianming jin, hardback, publisher: John Wiley and Sons  
Ltd Date of Publication 23/11/2010 ISBN-100470533595.
3. P. B. Johnson, and R. W. Christy, *Phys. Rev. B*, 1972, **6**, 4370–4379.
4. S. Bera, J. E. Lee, S. B. Rawal and W. I. Lee, *Appl. Cat. B: Environ.*, 2016, **199**, 55–63.
5. Q. H. Chen, S. N. Wu and Y. J. Xin, *Chem. Eng. J.*, 2016, **302**, 377–387.
6. Z. Wu, Q. Q. Fu, S. T. Yu, L. R. Sheng, M. Xu, C. Z. Yao, W. Xiao, X. Q. Li and Y. Tang, *Biosens. Bioelectron.*, 2016, **85**, 657–663.